Ceramics

Influence of stress on the electromechanical properties and the phase transitions of lead-free $(1 - x)Ba(Zr_{0.2}Ti_{0.8})O_3 - x(Ba_{0.7}Ca_{0.3})TiO_3$

Ahmed Gadelmawla[1,*] (iD), David Dobesh[1], Udo Eckstein[1], Oliver Grübl[1], Matthias Ehmke[2], Maria Rita Cicconi[1], Neamul H. Khansur[1], Dominique de Ligny[1], and Kyle G. Webber[1]

[1] *Department of Materials Science and Engineering, Friedrich-Alexander-Universität Erlangen-Nürnberg, 91058 Erlangen, Germany*
[2] *School of Materials Engineering, Purdue University, West Lafayette, IN 47907, USA*

ABSTRACT

The influence of stress on the phase boundaries of polycrystalline lead-free perovskite $(1 - x)Ba(Zr_{0.2}Ti_{0.8})O_3 - x(Ba_{0.7}Ca_{0.3})TiO_3$ (x = 0.4, 0.5, and 0.6) was characterized through the temperature- and stress-dependent small-signal dielectric and piezoelectric response from − 150 to 200 °C under uniaxial compressive stress up to − 75 MPa. For all three compositions, the phase transition temperatures separating the rhombohedral, orthorhombic, tetragonal, and cubic phases were shifted to higher temperatures with an increase in the uniaxial mechanical loading, corresponding to a significant decrease in the dielectric and piezoelectric responses. Additional stress-dependent relative permittivity measurements up to − 260 MPa were conducted at four different constant temperatures (− 10, 10, 25, and 40 °C), revealing significant increases in the dielectric response, making these materials interesting for tunable dielectric applications. Furthermore, the stress-induced shift in phase transition temperatures was confirmed by in situ combined temperature- and stress-dependent Raman spectroscopy measurements under different constant uniaxial loads within the temperature range from 30 to 130 °C.

GRAPHICAL ABSTRACT

σ-*T* dependent d_{33} σ-*T* phase diagram
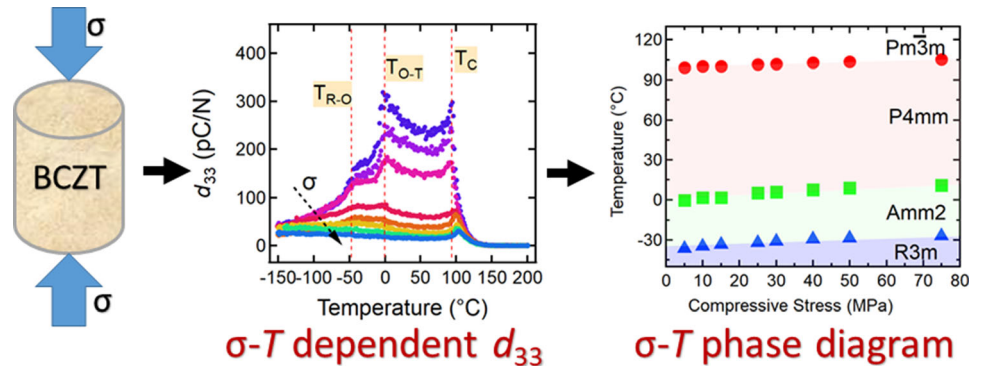
Introduction

Ferroelectrics continue to be an increasingly important material class for several technological sectors, as they are widely used in different electromechanical transducer applications, such as actuators, sensors, generators, and accelerometers [1–4]. Of all the lead-free ferroelectric materials [5–8] that have been developed to potentially replace lead zirconate titanate (Pb(Zr,Ti)O$_3$) (PZT) [5], Ba(Zr$_{0.2}$Ti$_{0.8}$)O$_3$–(Ba$_{0.7-}$Ca$_{0.3}$)TiO$_3$ (BCZT) has gained significant attention because of an exceptionally large piezoelectric coefficient $d_{33} \approx 620$ pC/N [13]. The origin of such high piezoelectricity is suggested to be related to the existence of a phase boundary that separates the rhombohedral *R3m* and tetragonal *P4mm* phases, as reported by Liu and Ren [9] as well as Haugen et al. [10]. In addition, the phase diagram also indicates a tricritical point of a paraelectric cubic phase (C, *Pm$\overline{3}$m*), ferroelectric rhombohedral (R, *R3m*), and ferroelectric tetragonal (T, *P4mm*) phases. Keeble et al.[11] and Damjanovic et al. [12] discussed the coexistence of the intermediate orthorhombic phase (O) with *Amm*2 space group, where they showed the presence of three phase transitions, i.e., R-O, O-T, and T-C, in the vicinity of room temperature. It is suggested that the polymorphism can enable a large piezoelectric response through the polarization rotation and extension mechanisms originating from a flattening of the energy landscape [9, 13]. The major limitations of the BCZT system, however, are the

relatively low Curie temperature T_C within a range of ∼ 70–120 °C depending on the Ca/Zr ratio [14] and the low mechanical stability, shown through a relatively low coercive stress of approximately − 5 MPa to − 20 MPa [15].

Understanding the influence of external mechanical and thermal fields on the functional properties of ferroelectrics is critical, as many applications expose the electroceramic component to large electrical, mechanical, and thermal fields during operation [5] that can change the observed electromechanical behavior [15], induce changes in the crystal structure or state [16–18], as well as lead to crack growth and potentially failure [19]. The influence of stress on the large- and small-signal electromechanical properties of normal ferroelectrics, such as PZT, Pb(Mg$_{1/3}$Nb$_{2/3}$)O$_3$–PbTiO$_3$, and (Pb$_{1-x}$La$_x$)(Zr$_{1-y}$Ti$_y$)O$_3$, has been investigated by several researchers, where the primary mechanism responsible for the observed macroscopic response is due to domain wall nucleation and growth [20–24]. Despite this, applied external electrical and mechanical fields have also been observed to induce structural phase transitions in polycrystalline perovskite ferroelectrics, such as PZT, PLZT, KNN, and BaTiO$_3$ [17, 25–29]. In particular, mechanical fields can significantly affect the stable phase in ferroelectric films, resulting in room temperature ferroelectricity in SrTiO$_3$ [30] and inducing a morphotropic phase boundary in BiFeO$_3$ [31]. In addition, lead-free relaxor ferroelectrics have revealed the stress-induced formation of long-range ferroelectric order [16, 32] related to the coalescence

of polar nano-regions into a periodic domain structure [33, 34].

The piezoelectric and dielectric responses observed in ferroelectric perovskites are comprised of both intrinsic and extrinsic contributions [35]. The intrinsic contribution originates from the electromechanical response of the crystal lattice and the extrinsic contribution due to other phenomena, such as the motion of domain walls and phase boundaries [36]. Both contributions can be influenced by external electrical, mechanical, and thermal fields [15, 37–39]. Here, simultaneously applied fields can either work with one another cooperatively or antagonistically, depending on the relative loading direction. Previous studies have investigated the effect of uniaxial compressive stress on the small-signal piezoelectric and dielectric response of $BaTiO_3$-based ceramics [40–42], which showed shifting in the Curie point to higher temperatures under uniaxial load. Furthermore, the change in the small-signal piezoelectric response of PZT under uniaxial stress was demonstrated [43–45]. For example, an initial increase in electromechanical coupling was reported in PZT, followed by a subsequent decrease with increasing stress due to an internal bias electric field induced by oriented defect dipoles working against an externally applied stress [37]. The Rayleigh coefficient α was demonstrated as a measure of domain wall motion irreversibility through stress-dependent Rayleigh measurements of numerous ferroelectrics, such as PZT and BT that displayed an increase in the piezoelectric coefficient with increasing dynamic stress [46]. In addition, an improvement in the direct piezoelectric response of PZT-Nb was observed with increasing dynamic stress up to 7 MPa under low static stress [47].

Despite the importance stress plays in ferroelectrics, the influence on lead-free ferroelectrics remains poorly understood. In particular, few studies have been presented on the mechanical properties of BCZT, although it shows excellent potential as a lead-free alternative and excellent electromechanical properties [42, 48]. The few available studies reveal a relatively low coercive stress in the range of − 5 MPa to − 20 MPa and a correspondingly low remanent strain, depending on composition [42, 49], suggesting enhanced mechanical depolarization in applications with a preload. In addition, uniaxial stress was found to significantly increase the large-signal electromechanical d_{33}^* of BCZT [42, 49], analogous to

observations in other ferroelectric material systems [50, 51]. Although the origins of the mechanical response remain unclear, previous studies by Ehmke et al. indicated that domain wall motion near the polymorphic phase boundary is primarily responsible for the hysteretic response [49, 52]. This is supported by in situ electric field-dependent X-ray diffraction data that demonstrates ferroelectric domain wall motion during application of an electric field [53]. Despite this, in situ transmission electron microscopy studies have shown an interesting single domain state during electrical loading [54], which suggests a transformation from a multiphase state to a purely orthorhombic phase. Similarly, in situ temperature-dependent PFM and Raman spectroscopy revealed the existence of a complex orthorhombic/rhombohedral nano-domains in a tetragonal matrix at room temperature [55]. Although the mechanism responsible for this mechanical behavior has not been directly observed through, e.g., in situ stress-dependent X-ray diffraction, the hysteretic mechanical response is understood to be primarily due to ferroelastic domain wall nucleation and growth as well as the influence of the multiphase state at room temperature in the vicinity of the polymorphic phase boundary [49, 52]. However, stress-modulated structural phase transitions have been observed in other $BaTiO_3$-based materials [56, 57], and it is not clear if such transitions influence the observed electromechanical response of BCZT.

Previous studies on BT, for example, focused exclusively on dielectric properties and the shifting of phase boundaries. This work presents the temperature-dependent piezoelectric coefficient across the three phase boundaries as a function of composition. Furthermore, the influence of applied stress on both the macroscopic small-signal electromechanical and dielectric response as well as the crystal structure of BCZT is presented as a function of temperature, demonstrating the role of external uniaxial compressive stress on the structural interferroelectric and ferroelectric-paraelectric phase boundaries. In addition, in situ Raman spectroscopy measurements were conducted as a function of temperature under uniaxial load. These data are used to develop a stress-temperature-composition phase diagram for BCZT as well as provide information on the reduction in extrinsic contributions to the electromechanical properties during mechanical loading. The experimental results are compared to previous studies on

BaTiO$_3$ to illustrate the effect of Ca and Zr substitution in the system. These data are crucial to developing and implementing the new lead-free electroceramics applications.

Experimental

Polycrystalline $(1 - x)$Ba(Zr$_{0.2}$Ti$_{0.8}$)O$_3$-x(Ba$_{0.7}$Ca$_{0.3}$)-TiO$_3$ (x = 40, 50, and 60 mol%, denoted as BCZT40, BCZT50, and BCZT60, respectively) samples were synthesized with a solid-state reaction method using analytical grade starting powders BaZrO$_3$ (99.5%, Sigma-Aldrich), CaCO$_3$ (99.0%, Sigma-Aldrich), BaCO$_3$ (99.8%, Alfa Aesar), and TiO$_2$ (99.8%, Sigma-Aldrich). The starting powders were ball-milled for 24 h in ethanol, dried in the air, and calcined for 2 h at 1350 °C. Sintering was carried out for 5 h in the air at 1450 °C. Additional details of the ceramic processing can be found elsewhere [58]. Sintered ceramics were ground into cylinders with a height of 6.00 ± 0.02 mm and a diameter of 5.80 ± 0.02 mm on a surface grinder, followed by an annealing step at 400 °C to depolarize the samples and remove any domains that may have been reoriented during sample preparation. All samples were sputtered with platinum electrodes on both circular faces with a thickness of approximately 70 nm. The samples were then poled in silicone oil for 30 min at room temperature with an electric field of 3 kV/mm [59]; measurements were performed at least 24 h after electrical poling.

A screw-type load frame (Instron 5967, Instron GmbH) with an integrated thermal chamber (TK 26.600.LN2, Fresenberger GmbH) was used for the stress-dependent electromechanical and dielectric characterization as a function of temperature. Additional information on the experimental arrangement can be found in previous works [37]. Two tungsten carbide loading dies were attached to the samples for uniaxial stress, which also acted as the electrical contacts. During measurement, a constant bias compressive stress between − 5 and − 75 MPa was maintained during heating from − 150 to 200 °C at a rate of 2 K/min; liquid nitrogen was used to cool the samples down to − 150 °C. The piezoelectric testing equipment is based on an integrated piezoelectric actuator that partially unloaded the sample using a sinusoidal waveform with an amplitude of ± 0.5 MPa at various frequencies between 0.5 and 140 Hz,

where a Sawyer–Tower circuit was used to determine the resulting change in polarization. Dielectric measurements were performed simultaneously with an attached LCR Meter (E4980AL, Keysight Technologies). A custom program was used to control, record, and analyze the obtained small-signal piezoelectric and dielectric data during heating [37]. Similarly, stress-dependent relative permittivity at 1 kHz was measured during compressive uniaxial stress loading within the range from − 1 to − 260 MPa with a loading/unloading rate of 0.25 MPa/s at selected constant temperatures, i.e., − 10, 10, 25, and 40 °C.

Raman spectra were acquired in the 38–1500 cm^{-1} frequency range using a coherent Sapphire SF single-frequency 488 nm laser (optical power 100 mW) as the excitation source, an *i*HR 320 Horiba monochromator coupled with a Sincerity UV–VIS CCD camera, and a custom-built optical microscope [60]. The 1800 lines/mm holographic grating and a 50 × microscope objective (OptoSigma PAL-50-L, NA 0.42) provided a spatial and frequency resolution of ∼ 1 µm and 2 cm^{-1}, respectively. A uniaxial load cell with a piezoelectric actuator equipped with ceramic resistive heaters was used for in situ stress- and temperature-dependent Raman spectroscopy measurements. Details of the setup can be found in our previous work [18]. A cuboid sample of BCZT60 with 3 mm × 2 mm × 2 mm dimensions was prepared from the cylinder sample with a diamond wire saw (WireTech GmbH & Co. KG) and a surface grinder. The BCZT sample was placed between two cuboid-shaped (2 mm × 2 mm × 2 mm) spacers made of ZrO$_2$ to minimize the thermal gradients upon heating. Conical loading pieces of tungsten carbide were used between the sample and the uniaxial load cell to ensure the uniformity of the applied stress and account for any minor misalignments. A K-type thermocouple was used to record the sample surface temperature during the measurements. In order to estimate the stress-dependent variation in Curie temperature from the Raman spectra collected at high temperatures, the data were reduced using the Bose–Einstein distribution. This procedure allows reducing the contributions from thermally populated excited vibrational states. Nevertheless, as a result, all temperature corrected (*T*-corrected) spectra show a suppression of the vibrations at low frequencies (see Figure S1, supplementary information). Therefore, temperature uncorrected signals are presented here. Raman signals were background-subtracted with a

linear function and normalized to the total area in the 40–1100 cm^{-1} frequency range.

Results and discussion

Temperature-dependent dielectric and piezoelectric behavior

The small-signal frequency-dependent relative permittivity ε_r and direct piezoelectric coefficient d_{33} of all three BCZT compositions were characterized from − 150 to 200 °C, allowing for the observation of the entire phase transition region separating the rhombohedral, orthorhombic, tetragonal, and cubic phases (Fig. 1). Although all compositions show three distinct phase transitions, it is important to note that the phase transition temperatures in BCZT40 are relatively close to each other compared to BCZT50 and BCZT60, indicating an enhanced phase coexistence in this composition. These results are consistent with previous reports [14, 61–63]. In order to maintain electrical and mechanical contact of the sample during testing, a constant uniaxial bias stress of − 5 MPa was applied during the experiment. The direct piezoelectric sufficient for all compositions was also determined at room temperature with a loading frequency of 110 Hz using a Berlincourt meter (Piezo-Meter, Piezotest Ltd) showing values of 258 ± 4 pC/N, 410 ± 2 pC/N, and 308 ± 5 pC/N for BCZT40, BCZT50, and BCZT60, respectively, which is good agreement with the measured value under uniaxial stress of − 5 MPa. This indicates that the applied bias stress of − 5 MPa did not significantly influence the electromechanical response of BCZT compositions, a result that is consistent with previous reports [37, 40]. As such, − 5 MPa was considered equivalent to the stress-free state during this investigation.

During heating, all compositions show piezoelectric and dielectric anomalies in the vicinities of the known structural phase transition temperatures, i.e., R-O, O-T, and T-C, at T_{RO}, T_{OT}, and T_C, respectively. In addition, the temperature difference between phase boundaries ΔT increased with Ca/Zr ratio, indicating an increasing thermal stability of the O and T phases. For example, the temperature range of the orthorhombic phase increased from approximately 15 °C in BCZT40 to 29 °C and 37 °C in BCZT50 and BCZT60, respectively. Similarly, the tetragonal phase stability increases from 17 to 50 °C

and 100 °C for BCZT40, 50, and 60, respectively. This is understood to be due to the polymorphic nature of the bridging phase boundary between the rhombohedral $BaZr_{0.2}Ti_{0.8}O_3$ and the tetragonal $Ba_{0.7}Ca_{0.3}TiO_3$ end members [10] as well as the increasing Curie temperature with enhanced tetragonality [11].

The piezoelectric coefficient displayed a sharp increase at all phase boundaries due to the well-known electrical and mechanical softening effects that occur during structural phase transitions, which corresponded well with the known dielectric response [11] (Fig. 1). It is important to note that despite the structural phase transformations at the R-O and O-T phase boundaries, the investigated BCZT compositions did not display a significant decrease in piezoelectric response through a loss in the poled domain structure. Interestingly, the maximum piezoelectric coefficient was found in all compositions at the interferroelectric phase transition temperature T_{OT}, where BCZT50 displayed the highest maximum d_{33} of 545 pC/N at 32 °C and BCZT40 and 60 had a maximum d_{33} of 515 pC/N at 54 °C and 385 pC/N at − 5 °C, respectively, whereas, in contrast, the maximum relative permittivity was observed in all compositions at the Curie point. Although the origins of this observation are unclear, it is likely due to the multiphase nature in this temperature region and the corresponding enhanced domain and phase wall mobility. Close to the phase boundary, the domain wall motion is thermally enhanced and that can result in lowering of the threshold stress required for switching, and an increase in the unit cell volume at higher temperature, consequently enhancing the extrinsic and intrinsic contributions [37, 64] to the macroscopic piezoelectric coefficient. The role of the bridging orthorhombic phase and the resulting O-T phase boundary was reported to enhance the elastic response and piezoelectric coupling of BCZT through an easing of the change of polarization direction [65]. Previous investigations have observed similar increases in the piezoelectric properties [5, 32], although the influence of interferroelectric phase transitions on the small-signal electromechanical properties, particularly in relation to the stability of the electrically induced domain state, is not well-understood.

The d_{33} values are expected to increase close to the phase boundaries as the d_{33} is coupled with the temperature dependence of relative permittivity ε'_{33}
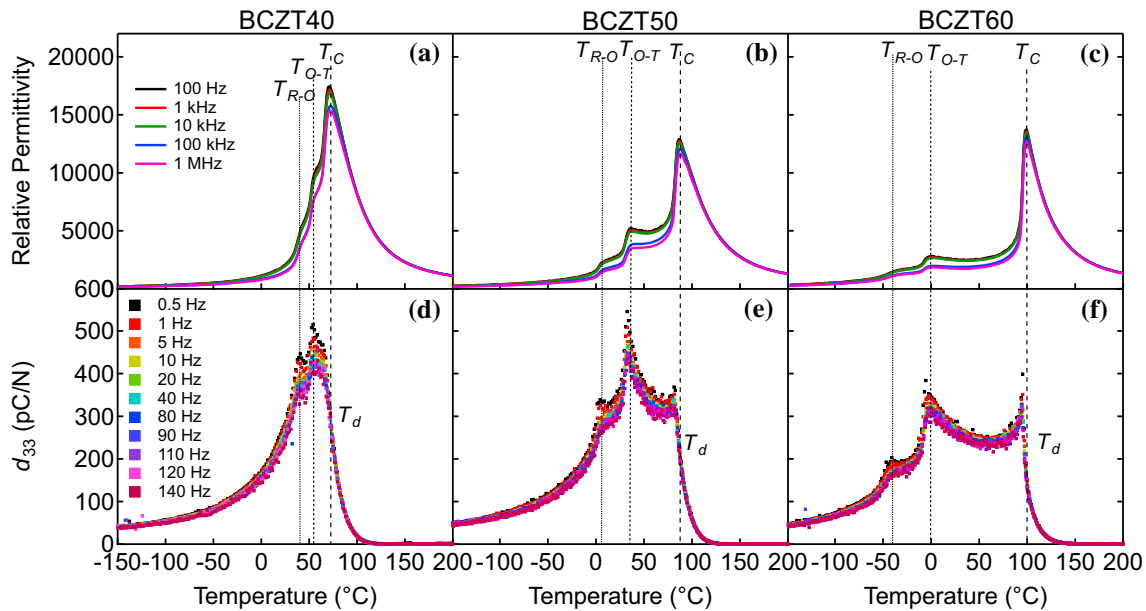
Figure 1 Relative permittivity (**a**, **b**, and **c**) and piezoelectric coefficient d_{33} (**d**, **e**, and **f**) at − 5 MPa of BCZT40, 50, and 60, respectively. Dotted and dashed lines represent R-O, O-T, Curie point T_C, and depolarization T_d temperatures.

and macroscopic polarization P_3 [66], as shown in Eq. 1:

$$d_{33} = 2Q_{11}P_3\varepsilon'_{33}\varepsilon_0 \tag{1}$$

where Q_{11} is the electrostrictive coefficient and ε_0 is the permittivity of vacuum. Assuming Q_{11} is independent of temperature [67, 68], a peak in the piezoelectric coefficient results from the significant increase in ε'_{33} and corresponding decrease in the macroscopic polarization at the ferroelectric-paraelectric phase boundary. The d_{33} peak, however, is limited at the Curie point due to the thermally induced loss of macroscopic polarization that causes a sharp decrease in electromechanical coupling. Interestingly, however, a sharp increase in the relative permittivity is not observed at the O-T phase boundary, despite the d_{33} peak, indicating that other extrinsic contributions, such as stress-induced phase transitions, can be playing an important role. Importantly, the polarization is not lost at interferroelectric phase boundaries, rather the thermally induced change in crystal symmetry alters the crystallographic direction and magnitude of the spontaneous polarization, influencing the local domain structure through changes in the domain wall type and density. In addition, as shown in Fig. 1, the depolarization temperature T_d can be represented by the inflection point in the sharp drop in d_{33} [37]. This

temperature corresponds well with the observed Curie point, which can be found as a peak in relative permittivity, indicating that T_C and T_d are the same temperature for the BCZT compositions investigated here. This observation is different than other studies, such as co-doped PZT and NBT, as the T_d was observed at lower temperatures than T_C [37, 69].

Stress- and temperature-dependent dielectric and piezoelectric behavior

The temperature-dependent d_{33} and ε_r were measured as a function of applied uniaxial compressive stress within the range from − 5 to − 75 MPa. As shown in Fig. 2, both the piezoelectric and the dielectric values decrease with increasing compressive stress, which is due to the reduction in domain wall density and mechanical depolarization of the sample as well as the increased clamping of domain wall motion with increasing applied uniaxial stress parallel to the poling direction [49]. Interestingly, however, the dielectric response was found to increase in all compositions in the rhombohedral phase in the vicinity of the R-O phase transition temperature. Although the origin of the behavior remains unclear, it is suggested to be due to the apparent dielectric peak broadening found at the dielectric anomalies at interferroelectric phase transitions as well as the maximum ε_r peaks at the Curie
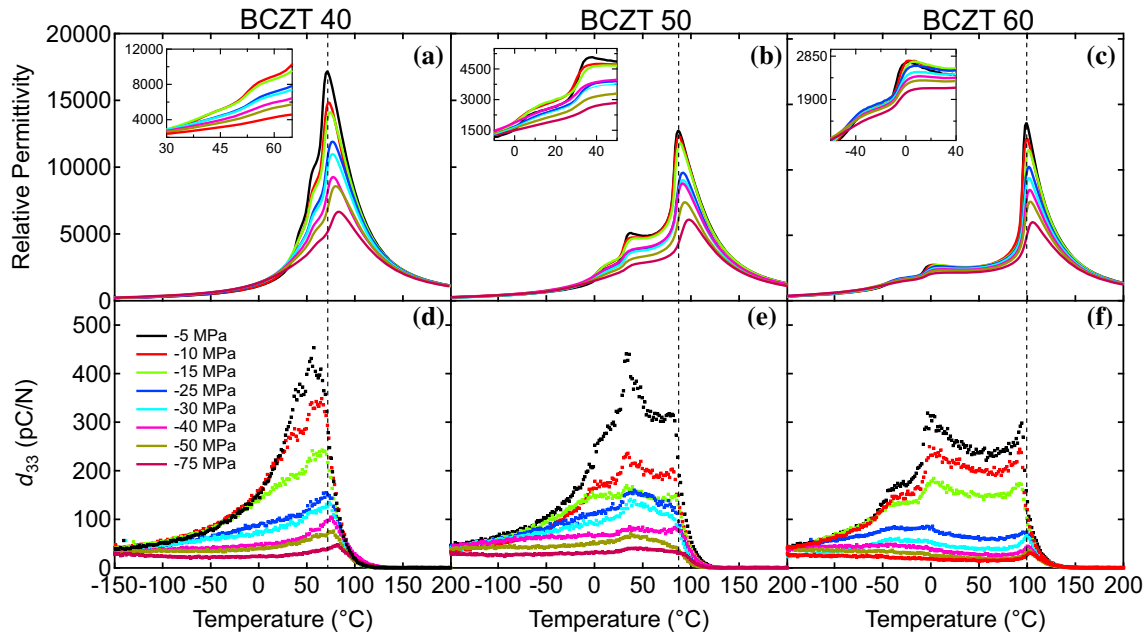
Figure 2 Temperature-dependent ε_r (10 kHz) (**a**, **b**, and **c**) and d_{33} (110 Hz) (**d**, **e**, and **f**) as a function of uniaxial compressive stress within the range from -5 to -75 MPa of BCZT40, 50, and 60, respectively. The inset figures represent the zoomed area of interferroelectric phase transitions respective to their compositions.

point with increasing compressive stress. A similar stress-dependent increase in the piezoelectric response was not observed, which would be expected in the case of a field-induced phase transition. This dielectric broadening is understood to be due to the random orientation of the grains and domains that display variations in the stress-dependent shift in the phase transition temperature [36, 40, 47]. At lower temperatures ranging from -150 to -125 °C, permittivity does not exhibit any significant variation with increasing applied stress for all compositions, indicating that the extrinsic contributions, such as domain wall motion, are significantly reduced at low temperature, resulting in a reduction in the both the macroscopic dielectric and piezoelectric properties as well as the stress sensitivity [70].

The interferroelectric and ferroelectric-paraelectric phase transition temperatures are found to shift with stress for all three compositions, corresponding well to previous observations in single crystal and polycrystalline BaTiO$_3$ [40, 41, 71–73]. Among the three investigated compositions, BCZT40 was found to be the most stress-sensitive, displaying a decrease in the maximum relative permittivity from -5 to -75 MPa of approximately 61%, in comparison with BCZT50 and 60 that showing decreases of 52% and 56%, respectively. This can be partially related to the

effect of Zr content on the structure and the associated variation in ionic radius between Zr^{4+} and Ti^{4+}, where Zr^{4+} (0.72 Å) is larger than Ti^{4+} (0.605 Å) [74]. The higher Zr content in the system, i.e., BCZT40, causes less phase stability due to internal chemical pressure in the unit cell, and therefore phase boundaries are more sensitive to the applied stress [38, 75–81]. Thus, the change in the small-signal response under stress for the different BCZT compositions, i.e., 40, 50, and 60, shows a good correlation with the reported Young's moduli for these compositions [49]. By comparison, BCZT60 reported the highest elastic modulus and coercive stress compared to BCZT40 and 50.

Similarly to the relative permittivity, all compositions display a significant decrease in the temperature-dependent piezoelectric response with increasing uniaxial compressive stress, consistent with previous investigations on PZT and NBT-BT [32, 37]. At -5 MPa, an anomaly in the piezoelectric coefficient can be seen at phase transitions, corresponding to those found in the dielectric behavior. With increasing stress, however, these anomalies are reduced in intensity, where at above approximately -30 MPa they can no longer be observed for any composition despite their continued appearance in the temperature-dependent dielectric
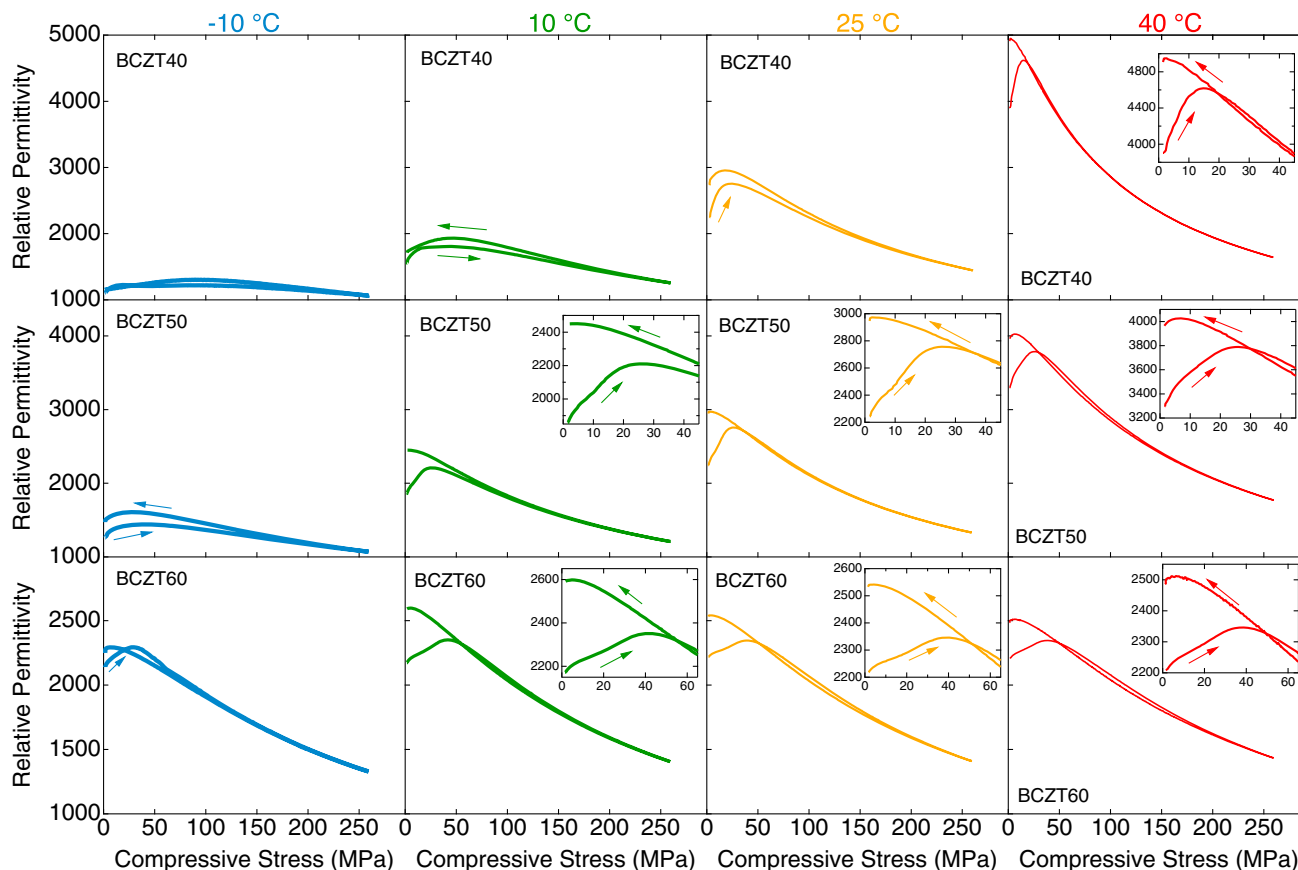
Figure 3 Stress-dependent relative permittivity for BCZT40, 50, and 60 at − 10 °C, 10 °C, 25 °C, and 40 °C. The measurement frequency was 1 kHz. The arrows refer to the loading and unloading directions.

measurements. In contrast to the observed dielectric behavior, an increase in d_{33} in the vicinity of the R-O phase transition was not observed. It is interesting to note that even at the highest applied stress, there remains a piezoelectric response, meaning that the macroscopic polarization is retained up to − 75 MPa. In BCZT40 case, the decrease in the maximum d_{33} from − 5 to − 75 MPa was approximately 92%, whereas, in BCZT50 and BCZT60, the decreases were 91% and 94%, respectively. Such a decrease in the d_{33} values under stress make the material inadequate for high load applications. In addition, these data also show a clear temperature dependence in the stress sensitivity of the piezoelectric behavior. At temperatures above approximately − 50 °C, there is a significant decrease in d_{33} with increasing stress, whereas at − 150 °C, all materials display a piezoelectric response nearly independent of the applied stress. In analogy with the dielectric properties, this is also due to the reduced extrinsic contributions to the

electromechanical properties at lower temperatures from decreased thermal energy.

In order to investigate the observed stress-dependent increase in the relative permittivity (Fig. 2), stress-dependent relative permittivity (1 kHz) was measured up to − 260 MPa at four constant temperatures (− 10, 10, 25, and 50 °C) from the unpoled state, as shown in Fig. 3. The temperatures were selected to represent different phase regions of each composition. Importantly, for all compositions and temperatures, the relative permittivity values initially increased before decreasing with increasing stress. Subsequently, during unloading, the remanent relative permittivity was found to increase above the original unloaded value for all materials and temperatures. It is well-known that the dielectric properties of ferroelectric materials are not isotropic, clearly shown in the classic investigation by Merz, where he found a significantly larger dielectric response of a-axis oriented BaTiO$_3$ domains compared to c-axis oriented domains [82]. In the present

study, mechanical loading can lead to an increase in the number of *a*-axis oriented domains parallel to the axis of applied uniaxial stress. At lower stress levels, where mechanical domain clamping remains limited, this reorientation can increase the apparent relative permittivity by breaking the initial isotropic symmetry of the polycrystalline materials. However, the subsequent decrease with increasing stress is due to a stress-induced decrease in the extrinsic contributions to the dielectric response, e.g., domain wall clamping. A similar effect has been observed in PZT [37], BT [40], and BCZT [5].

At − 10 °C, BCZT40 and 50 both display a broader stress-dependent relative permittivity, which is due to the low extrinsic contribution on the domains switching at lower temperatures; both of these compositions are in the rhombohedral phase at this temperature, where a reduced stress sensitivity was observed (Fig. 2). With increasing temperature into the orthorhombic and tetragonal phases, however, sharper dielectric peaks are observed with increasing stress, followed by a subsequent decrease. This is consistent with an increase due to enhance *a*-axis orientation of domains parallel to the applied stress direction. Despite this, however, stress-induced structural phase transitions are also possible and have been observed in other perovskite ferroelectrics [56, 57, 83]. For example, a change in the slope of the stress-dependent permittivity is observed at approximately − 6 MPa in BCZT50 during mechanical loading at 40 °C, which can potentially be related to an O-T phase transition [5] or due to the field-induced single domain state [54, 84, 85]. Here, additional in situ structural investigations, such as stress-dependent synchrotron X-ray diffraction or transmission electron microscopy, are required to determine the mechanism responsible and the stress effect on the polymorphic phase boundaries and domain switching.

Temperature-stress phase diagram

As shown in Fig. 2, uniaxial compressive stress results in a significant change in the relative permittivity, marked by a shift in the dielectric anomalies at the three structural phase boundaries present, i.e., the dielectric anomalies around the phase transition temperatures are broadened and shifted to higher temperatures. In order to quantify this stress-dependent shift, the phase transition temperatures were

extracted from the derivative of the permittivity data as a function of temperature (Fig. 4), allowing for the construction of a temperature-stress phase diagram. Such a phase diagram provides important information in evaluating the stability region of functional properties under combined stress and thermal field. Under − 5 MPa uniaxial stress, all compositions show three peaks representing the different transitions, i.e., R-O, O-T, and T-C, at approximately 40 °C, 45 °C, and 71 °C for BCZT40; 5 °C, 34 °C, and 86 °C for BCZT50; and − 36 °C, 0 °C, and 100 °C for BCZT60, respectively, corresponding well to previous studies [12, 14, 62, 63]. However, with increasing compressive stress, all peaks display broadening, a significant decrease in the maximum permittivity
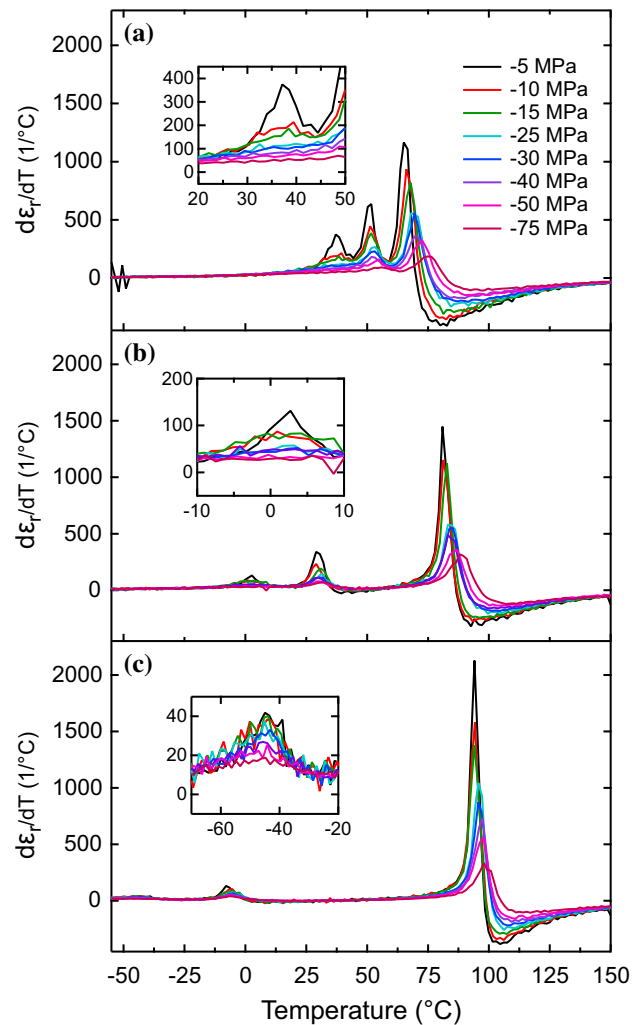

Figure 4 Change in permittivity as a function of temperature $d\varepsilon_r/dT$ is drawn versus temperature T for **a** BCZT40, **b** BCZT50, and **c** BCZT60. Insets magnify the R-O phase transition for each composition.

value, and a shift to higher temperatures, where the magnitude of the change is related to the exact phase transition boundary and the applied stress. For example, BCZT60 displays three clear peaks at the respective phase transitions for all investigated compressive stress values. In contrast, the R-O phase transition in both BCZT50 and BCZT40 is no longer visible within the resolution of these measurements after − 40 MPa and − 30 MPa, respectively, which could be related to reported higher coercive stress of the tetragonal phase compared to the other phases [49].

The temperature-stress phase diagram of BCZT40, BCZT50, and BCZT60 as a function of constant uniaxial compressive stress in the range of − 5 MPa to − 75 MPa are presented in Fig. 5. The observed variation in transition temperature for each composition for the pre-stress condition corresponds well with previously reported phase diagrams [12, 14]. Importantly, the R-O, O-T, and T-C phase transition temperatures were found to increase in all compositions approximately linearly with increasing stress. For BCZT40, 50, and 60, the R-O phase boundaries displayed the most significant composition-dependent change in the linear slope, with values of 0.34, 0.23, and 0.13 K/MPa, respectively. The O-T phase boundaries were found to have linear slope values of 0.14, 0.10, and 0.16 K/MPa, respectively, and the stress-dependent Curie point revealed linear change of 0.16, 0.15, and 0.09 K/MPa, respectively. Both the O-T and T-C phase boundaries change rates are approximately constant within the resolution of the measurements. In comparison, the change in Curie point under uniaxial compressive stress was reported for polycrystalline and single crystal BT of 0.02–0.05 K/MPa and 0.19 K/MPa, respectively [40]. The relatively higher values of polycrystalline BCZT compared to polycrystalline BT can be related to the substitution in the A and B sites with different size cations, i.e., Ca and Zr [86, 87]. The composition-dependent variations in slopes indicate the different degrees of mechanical phase stability under compressive stress and are possibly related to the changes in unit cell volume, which is due to the change in the Zr to Ca content. Therefore, the slope values increase with increasing Zr content on the B-site, as the larger size of Zr ions leads to more internal pressure in the unit cell and reduced phase stability [14, 79, 80]. Furthermore, introducing smaller Ca cations in the A-site is found to significantly decrease the extent of
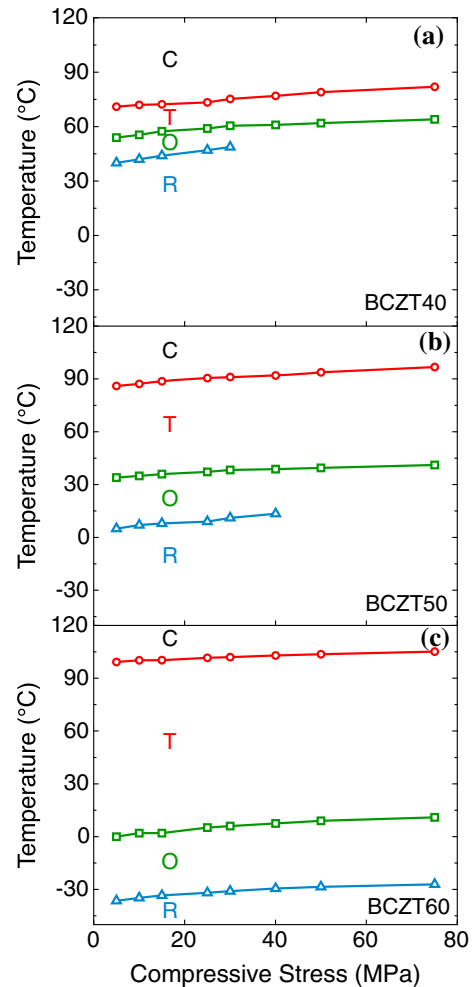

Figure 5 Temperature-stress phase diagram of polycrystalline **a** BCZT40, **b** BCZT50, and **c** BCZT60 as functions of constant uniaxial compressive stress (from − 5 to − 75 MPa).

the stress-induced Curie temperature shift. A similar effect was reported for Li doped KNN under compressive stress, where the increase in smaller Li cations on the A-site leads to a reduction in the stress-induced T-C phase transition from 0.119 to 0.092 K/MPa for LKNN0 and LKNN2, respectively [88].

As shown in Figs. 2 and 4, after − 30 MPa and − 40 MPa in BCZT40 and 50, respectively, the determination of the onset point of the R-O phase transition was indistinguishable as the peaks broadened and flattened with stress. A similar effect has been observed for R-O phase transition with stress in BaTiO$_3$ [57]. In addition, the slope of the R-O phase boundary in BCZT40 and 50 shows a significantly higher linear slope, indicating that with further

increasing stress, the R-O phase boundary intersects the O-T phase boundary, effectively eliminating the O-phase and resulting in a new R-T phase boundary. Assuming a continuing linear change with stress, BCZT40 and BCZT50 would show an intersection and subsequent elimination of the O-phase at − 81 MPa and − 238 MPa, respectively. Analogously, there has been considerable research into the formation of an R-T phase boundary in lead-free ferroelectric, such as $(K,Na)NbO_3$-based compositions, through the chemical substitution to eliminate the O-phase [89, 90]. These works have revealed an enhancement in the electromechanical properties as well as improved temperature stability. These data suggest that stress tuning might have similar effects due to the relative mechanical stability of different phase boundaries [17, 88]. Comparable changes in the phase boundaries for $BaTiO_3$ have been reported under pressure by Hayward and Salje [91], which has shown a possible R–C phase transition for $BaTiO_3$ beyond a critical point at 6.5 GPa. Additional structural studies, such as in situ stress-dependent XRD and TEM, would be required to illustrate the phase transitions under load.
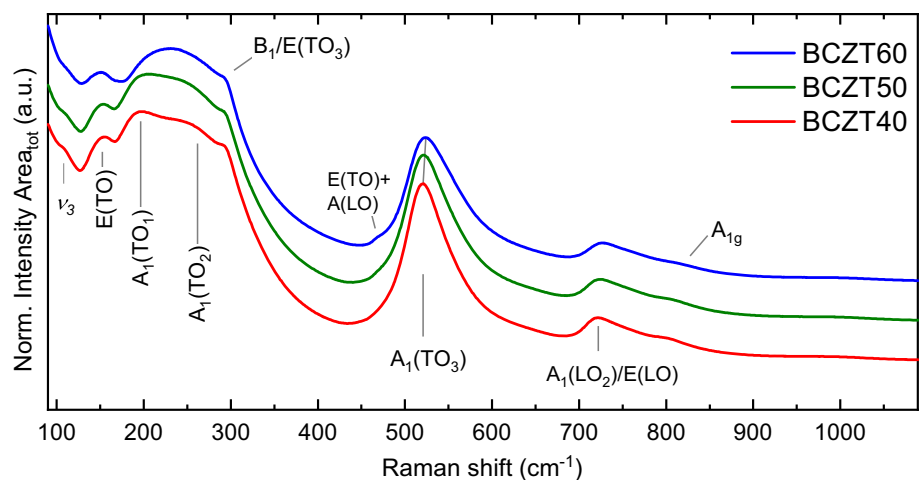
Stress- and temperature-dependent Raman spectroscopy

To investigate the variation in the local structure under combined stress and temperature loading, in situ stress- and temperature-dependent Raman spectroscopy was performed with a custom-built sample stage [18]. Despite being a surface-sensitive technique, Raman spectroscopy provides critical information on the local structural changes in functional ceramics [92, 93]. As such, the room temperature local structure of all three compositions were investigated to gain insight on the influence of varying Ca/Ba and Zr/Ti contents. Figure 6 shows the room temperature Raman spectra of the three samples. There are several relatively broad vibrations representing stretching of the <Ti–O> bond in TiO_6-octahedra as well as bending modes of the Ti–O–Ti bonds and vibrations of the A-site cations against the TiO_6-octahedra at low frequencies (< 100 cm^{-1}, v_3), in agreement with previous assignments of the first-order Raman bands in perovskite-type structures [94–96].

The main vibrations observed in Fig. 6 are transverse (TO) and longitudinal (LO) modes at $\sim$ 150, 193, 253, 293, 470, 522, 720, and 800 cm^{-1} associated with $E(TO_1)$, $A_1(TO_1)$, $A_1(TO_2)$, $B_1/E(TO_2)$, $A_1(TO_3)$, $E(TO) + A(LO)$, $A_1(LO_2)/E(LO)$, and A_{1g} modes, respectively, according to previous reports [97, 98]. Depending on the perovskite structure, there are characteristic bands previously used as fingerprints, such as the $A_1(TO_{1,2})$ vibrational modes in the frequency range $\sim$ 190–250 cm^{-1} that should indicate the stabilization of the rhombohedral phase in perovskites [99, 100]. In contrast, the presence of a relatively sharper mode at $\sim$ 293 cm^{-1} and a shoulder contribution at $\sim$ 470 cm^{-1} ($(E(TO) + A(LO))$) have been associated with tetragonal and orthorhombic phases, respectively [101]. The disappearance of the B_1 mode at $\sim$ 293 cm^{-1} and the suppression of the band at $\sim$ 720 cm^{-1} are usually associated with the transition from ferroelectric to paraelectric [101–103]. The observed variations in the band shapes, positions, and relative intensities of the Raman modes at room temperature (Fig. 6) are directly related to

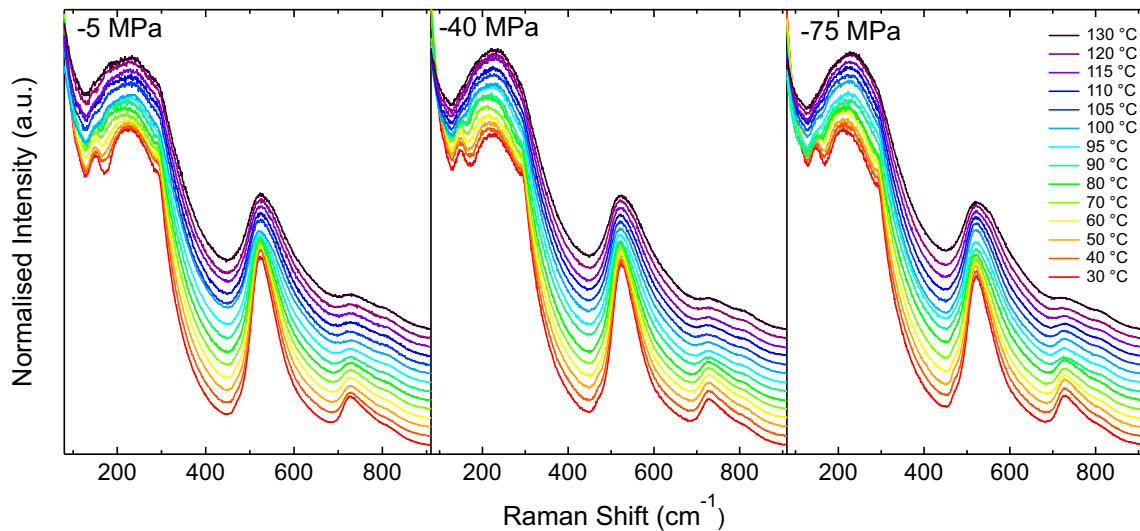**Figure 6** Normalized Raman spectra of BCZT40, 50, and 60 ceramics, collected at room temperature.

Figure 7 In situ Raman stress-temperature-dependent spectra of BCZT60 under uniaxial stresses of − 5 MPa, − 40 MPa, and − 75 MPa.

varying degree of Ca and Zr contents in the samples and in turn, with the different phases, in agreement with previous reports [104].

Due to the limitation of the experimental arrangement, in situ stress and temperature-dependent Raman spectroscopy measurements are limited to between room temperature and 400 °C [18]. As BCZT40 and BCZT50 both show multiple phase transitions above room temperature within proximity of each other (Fig. 1), separating the stress-dependent effects of these phase boundaries with the experimental arrangement used here is challenging. As such, we focus on the BCZT60 composition to show the influence of stress on the local structure, as it presents a single-phase transition (T-C) above room temperature. The variations in temperature-dependent Raman spectra under different uniaxial stress of − 5 MPa, − 40 MPa, and − 75 MPa in BCZT60 are shown in Fig. 7. The evolution of the Raman spectra with increasing temperature shows a continuous decrease in the intensities of the main peaks and a general broadening of all modes. Furthermore, by increasing the temperature, the $A_1(TO_2)$ band at ~ 200 cm^{-1} linearly shifts toward lower frequencies (see Fig. S1, S2, and S3). At high temperatures (> 110 °C), it is clear that the Raman spectra show only two main broad vibrations centered at ~ 228 cm^{-1} and ~ 520 cm^{-1}, typical features of the paraelectric cubic phase [55, 79, 105].

Upon increasing the stress, the bands at lower frequencies (< 360 cm^{-1}) do not change their position

significantly, and all seem unaffected by the applied uniaxial compressive stress, except the $A_1(TO_{1-2})$ modes. On the contrary, the bands at higher frequencies (> 400 cm^{-1}) show clear changes with increasing stress. Specifically, the strong contribution of $A_1(TO_3)$ at ~ 520 cm^{-1} and the shoulder E(TO) + A(LO) at 468 cm^{-1} display significant variation for the maximum applied stress of − 75 MPa, however only for temperatures lower than 100 °C, after which the $A_1(TO_3)$ vibrations are identical, suggesting, at first glance, the stabilization of a similar <Ti–O> bonding environment. However, at 100 °C, the A(LO)/E(LO) mode (720 cm^{-1}) still exhibits variation depending on the stress. These observations highlight that different applied stresses influence the <Ti–O> bonding environment in TiO$_6$ octahedra differently.

Previous works have used several different methods for analyzing temperature-dependent Raman spectroscopy data to estimate the phase transition temperatures [79, 106, 107]. For example, the $E(TO_2)$ mode (at ~ 150 cm^{-1} at RT) frequency shifts can be related to O-T and T-C phase transitions, according to various studies [79, 106, 107]. In BaTiO$_3$, it was observed that the bands at ~ 305 and ~ 715 cm^{-1} are strongly suppressed above the Curie temperature [108]. Another method to extract structural information from the Raman signals involves the deconvolution of the bands. This procedure should allow following the variations of the band relative intensities, width, and frequency positions, e.g., with change

in temperature [55]. However, the overlap of a large number of broad bands associated with the perovskite vibrations requires many assumptions on bandwidth and intensity/frequency variations, especially when changing temperature and phase. Therefore, the deconvolution of the whole Raman signal is considered unreliable. Furthermore, dielectric measurements show that the interferroelectric phase transitions, i.e., R-T and O-T, were less sensitive to the applied stress and not readily distinguishable (see Sect. 3.2.). As a result, the Raman data analysis methods previously carried out do not provide a fixed model to define such diffuse ferroelectric phase transitions. Nevertheless, the transition from the ferroelectric to the paraelectric phase is highly sensitive to stress and could be determined from stress- and temperature-dependent Raman spectroscopic data. For instance, in Fig. 7, it is evident that the change of the intensity of the $A_1(LO_2)/E(LO)$ mode (~ 720 cm^{-1}) follows the increase in temperature and could be used to detect the shifts in Curie temperature [101–103]. As such, by tracking the relative intensity variations occurring in the high-frequency bands (650–900 cm^{-1}) with temperature under different constant applied stresses, it might be possible to highlight the stress-induced variation in tetragonal to cubic phase transition temperature.

A continuous variation of most of the bands was observed upon temperature and stress increase, particularly a steady intensity decrease in the modes at 150 and 293 cm^{-1}, making them not particularly efficient to identify the T-C transition (Fig. S2). On the contrary, the change in relative peak intensities of the high-frequency bands (650–900 cm^{-1}) can be considered as an indication of a stress-induced change in phase stability. We considered different approaches, and the best approach was the deconvolution of the background-subtracted modes in the high-frequency region. In this approach, the different contributions (mathematical functions) have been identified by using the second derivative of the spectra, and three Gaussian functions are needed (Fig. S3). The barycenter of the whole high-frequency region has been determined by taking into account the frequency position of each Gaussian function (G, cm^{-1}) and its integrated area (A), according to Eq. 2:

$$\text{Barycenter}\left(\text{cm}^{-1}\right) = \frac{\sum(G_n \bullet A_n)}{A_{\text{tot}}} \quad (2)$$

More straightforward results are provided by the evolution of the barycenter, which is reported in Fig. 8 as a function of temperature for constant applied stress of -5 MPa, -40 MPa, and -75 MPa. The barycenter trends show similar, but not identical behavior, with a sudden increase of the frequency position occurring for temperatures higher than 80 °C. Upon heating under -5 MPa stress, the barycenter shows a steady change up to 80 °C, followed by a relatively steep increase up to 100 °C and an apparent saturation plateau. Similarly, for increasing applied stresses, a minor continuous change of the barycenter is observed by increasing the temperature up to 80 °C. However, for higher temperatures, changes in the slope are visible. The Curie temperatures determined using the temperature-dependent dielectric behavior match well with the changes observed in the barycenter. Therefore, there is a good agreement between Raman and the macroscopic stress-dependent dielectric properties (Fig. 5).

Different applied stresses cause a different response in the Raman vibrations (see also Fig. S2 and S3). The sudden damping of the mode at ~ 720 cm^{-1} at approximately 80 °C has been previously assigned to the transition to the cubic phase [109]. However, at the same time, in the Raman

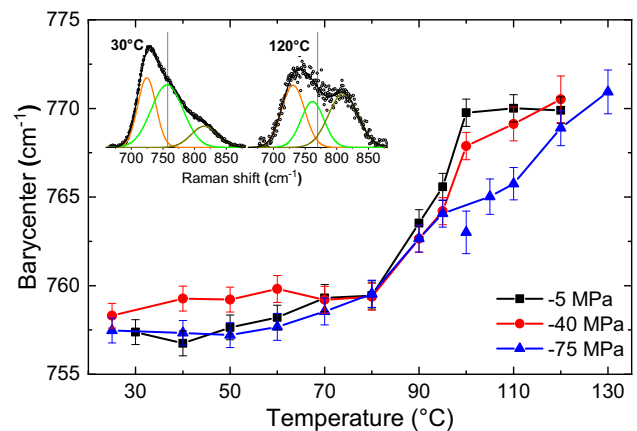**Figure 8** Barycenter of the high-frequency region (650–900 cm^{-1}) of sample BCZT60 as a function of temperature under different uniaxial loads of -5 MPa, -40 MPa, and -75 MPa. The phase region boundaries identified from the macroscopic dielectric measurements are consistent with the main slope changes observed here. In the inset, examples of the deconvoluted bands, where the Barycenter is represented with a vertical line.

spectra, there are vibrational bands considered a signature of the tetragonal phase, e.g., the shoulder E(TO) + A(LO) at 468 cm^{-1} and the B_1 mode at $\sim$ 290 cm^{-1}. In particular, the latter vibration suggests asymmetry within the TiO6-octahedra, indicating a tetragonal structure [110]. Therefore, the coexistence of tetragonal and cubic phases is suggested for all applied stresses, starting from $\sim$ 80 °C. Consequently, the first significant slope-change in the barycenter should be related to the presence of a polymorphic phase boundary, in agreement with previous studies [49, 52] and the macroscopic measurements. Based on these observations, the different trends of the barycenter are proposed to represent three different phase regions, namely tetragonal (plateau below 80 °C), tetragonal + cubic ($T \geq 80$ °C), and cubic phases ($T \geq 100$ or 105 °C, depending on the stress). As a result, the phase boundaries identified from the macroscopic dielectric measurements are consistent with the main variations observed by in situ Raman spectroscopy. In particular, the barycenter evolution for low and high applied stresses suggests that there is small positive increase in the T_C by increasing stress and, therefore, the phase boundary in polycrystalline BCZT is shifted by applying compressive stress, a result consistent with previous reports [40, 57].

Conclusions

In summary, the effect of uniaxial compressive stress on the relative permittivity and piezoelectric coefficient of $(1 - x)$Ba(Zr$_{0.2}$Ti$_{0.8}$)O$_3$–x(Ba$_{0.7}$Ca$_{0.3}$)TiO$_3$ (x = 0.4, 0.5, and 0.6) was characterized from − 150 °C to 200 °C with constant stress steps from − 5 MPa to − 75 MPa. The increasing compressive stress was found to suppress both the relative permittivity and piezoelectric coefficient due to domain wall clamping and corresponding decreasing extrinsic contributions. In contrast, permittivity data showed a significant shift of the phase transition temperatures with increasing stress and a broadening of the permittivity-temperature peaks around phase boundaries as a result of phase stability changes. At low temperature, the extrinsic contribution due to mechanical loading is insignificant, resulting in an approximately stress-invariant dielectric and piezoelectric response. Stress-dependent Raman spectroscopy data collected as a function of temperature

confirm the shift in Curie temperature under uniaxial load in BCZT60, corresponding well to the stress-dependent dielectric behavior. This work provides important information on the stability of dielectric and piezoelectric properties of BCZT-based compositions under combined compressive stress and temperature field.

Declarations

Conflict of interest The authors declare no conflict of interest.

Supplementary Information: The online version contains supplementary material available at https://doi.org/10.1007/s10853-022-07685-9.

References

[1] Carter CB, Norton MG (2007) Ceramic materials: science and engineering 716. Springer

[2] Moulson AJ, Herbert JM (2003) Electroceramics: Materials, properties, applications. Wiley, New York

[3] Cook WR, Jaffe H, Jaffe B (1971) Piezoelectric ceramics

[4] Uchino K (2009) Ferroelectric devices 2nd Edition, 2nd edn. Taylor and Francis, Hoboken

[5] Webber KG, Vögler M, Khansur NH, Kaeswurm B, Daniels JE, Schader FH (2017) Review of the mechanical and fracture behavior of perovskite lead-free ferroelectrics for actuator applications. Smart Mater Struct. https://doi.org/10.1088/1361-665X/aa590c

[6] Shrabanee Sen RNP, Choudhary (2004) Effect of doping Ca ions on structural and electrical properties of Ba(Zr 0.05 Ti 0.95)O 3 electroceramics. J Mater Sci Mater Electron https://doi.org/10.1023/B:JMSE.0000038922.74021.d6

[7] Li J-F, Wang K, Zhu F-Y, Cheng L-Q, Yao F-Z (2013) (K, Na)NbO 3 -based lead-free piezoceramics: fundamental aspects, processing technologies, and remaining challenges. J Am Ceram Soc. https://doi.org/10.1111/jace.12715

[8] Rödel J, Jo W, Seifert KTP, Anton E-M, Granzow T, Damjanovic D (2009) Perspective on the development of lead-free piezoceramics. J Am Ceram Soc. https://doi.org/10.1111/j.1551-2916.2009.03061.x

[9] Liu W, Ren X (2009) Large piezoelectric effect in Pb-free ceramics. Phys Rev Lett. https://doi.org/10.1103/PhysRevLett.103.257602

[10] Bjørnetun Haugen A, Forrester JS, Damjanovic D, Li B, Bowman KJ, Jones JL (2013) Structure and phase transitions in 0.5(Ba 0.7 Ca 0.3 TiO 3)-0.5(BaZr 0.2 Ti 0.8 O 3) from − 100 °C to 150 °C. J Appl Phys. Doi:https://doi.org/10.1063/1.4772741

[11] Damjanovic D, Biancoli A, Batooli L, Vahabzadeh A, Trodahl J (2012) Elastic, dielectric, and piezoelectric anomalies and Raman spectroscopy of 0.5Ba(Ti 0.8 Zr 0.2)O 3 -0.5(Ba 0.7 Ca 0.3)TiO 3. Appl Phys Lett Doi:https://doi.org/10.1063/1.4714703

[12] Keeble DS, Benabdallah F, Thomas PA, Maglione M, Kreisel J (2013) Revised structural phase diagram of (Ba 0.7 Ca 0.3 TiO 3)-(BaZr 0.2 Ti 0.8 O 3). Appl. Phys. Lett. Doi:https://doi.org/10.1063/1.4793400

[13] Damjanovic D (2010) A morphotropic phase boundary system based on polarization rotation and polarization extension. Appl Phys Lett. https://doi.org/10.1063/1.3479479

[14] Bai Y, Matousek A, Tofel P, Bijalwan V, Nan B, Hughes H, Button TW (2015) (Ba, Ca)(Zr, Ti)O3 lead-free piezoelectric ceramics—The critical role of processing on

properties. J Eur Ceram Soc. https://doi.org/10.1016/j.jeurceramsoc.2015.05.010

[15] Brandt DRJ, Acosta M, Koruza J, Webber KG (2014) Mechanical constitutive behavior and exceptional blocking force of lead-free BZT- x BCT piezoceramics. J Appl Phys. https://doi.org/10.1063/1.4879395

[16] Martin A, Uršič H, Rojac T, Webber KG (2019) Direct observation of the stress-induced domain structure in lead-free (Na 1/2 Bi 1/2)TiO 3 -based ceramics. Appl Phys Lett. https://doi.org/10.1063/1.5084255

[17] Khansur NH, Martin A, Riess K, Nishiyama H, Hatano K, Wang K, Li J-F, Kakimoto K, Webber KG (2020) Stress-modulated optimization of polymorphic phase transition in Li-doped (K, Na)NbO 3. Appl Phys Lett. https://doi.org/10.1063/5.0016072

[18] Khansur NH, Eckstein UR, Bergler M, Martin A, Wang K, Li J-F, Cicconi MR, Hatano K, Kakimoto K, Ligny D, Webber KG (2021) In situ combined stress- and temperature-dependent Raman spectroscopy of Li-doped (Na, K)NbO 3. J Am Ceram Soc. https://doi.org/10.1111/jace.18269

[19] Mishra R, Burela RG (2019) Thermo-electro-mechanical fatigue crack growth simulation in piezoelectric solids using XFEM approach. Theoret Appl Fract Mech. https://doi.org/10.1016/j.tafmec.2019.102388

[20] von Cieminski J, Diestelhorst M, Beige H (1989) Complex investigations of electrostrictive PMN-ceramics. Ferroelectrics. https://doi.org/10.1080/00150198908017362

[21] Kerkamm I, Hiller P, Granzow T, Rödel J (2009) Correlation of small- and large-signal properties of lead zirconate titanate multilayer actuators. Acta Mater. https://doi.org/10.1016/j.actamat.2008.08.057

[22] Liu Y, Ling Z, Zhuo Z (2017) High piezoelectricity of PLZT ceramics with strong frequency-dielectric dispersion below depolarization temperature. J Alloy Compd. https://doi.org/10.1016/j.jallcom.2017.08.113

[23] Chaplya PM, Carman GP (2002) Compression of piezoelectric ceramic at constant electric field: Energy absorption through non-180° domain-wall motion. J Appl Phys. https://doi.org/10.1063/1.1489498

[24] Lynch CS (1996) The effect of uniaxial stress on the electro-mechanical response of 8/65/35 PLZT. Acta Mater. https://doi.org/10.1016/S1359-6454(96)00062-6

[25] Hinterstein M, Hoelzel M, Kungl H, Hoffmann MJ, Ehrenberg H, Fuess H (2011) In situ neutron diffraction study of electric field induced structural transitions in lanthanum doped lead zirconate titanate. Z Kristallogr. https://doi.org/10.1524/zkri.2011.1338

[26] Hinterstein M, Rouquette J, Haines J, Papet P, Knapp M, Glaum J, Fuess H (2011) Structural description of the

macroscopic piezo- and ferroelectric properties of lead zirconate titanate. Phys Rev Lett. https://doi.org/10.1103/PhysRevLett.107.077602

[27] Martin A, Kakimoto K, Hatano K, Doshida Y, Webber KG (2017) Ferroelastic behavior across the orthorhombic-to-tetragonal phase transition region of NKN-based lead-free ferroelectrics. J Appl Phys. https://doi.org/10.1063/1.4989759

[28] Seo Y-H, Franzbach DJ, Koruza J, Benčan A, Malič B, Kosec M, Jones JL, Webber KG (2013) Nonlinear stress-strain behavior and stress-induced phase transitions in soft Pb(Zr 1–x Ti x)O 3 at the morphotropic phase boundary. Phys Rev B. https://doi.org/10.1103/PhysRevB.87.094116

[29] Daniels JE, Picht G, Kimber S, Webber KG (2013) Mechanical double loop behavior in BaTiO 3 Stress induced paraelastic to ferroelastic phase transformation. Appl Phys Lett. https://doi.org/10.1063/1.4821446

[30] Haeni JH, Irvin P, Chang W, Uecker R, Reiche P, Li YL, Choudhury S, Tian W, Hawley ME, Craigo B, Tagantsev AK, Pan XQ, Streiffer SK, Chen LQ, Kirchoefer SW, Levy J, Schlom DG (2004) Room-temperature ferroelectricity in strained SrTiO3. Nature. https://doi.org/10.1038/nature02773

[31] Zeches RJ, Rossell MD, Zhang JX, Hatt AJ, He Q, Yang C-H, Kumar A, Wang CH, Melville A, Adamo C, Sheng G, Chu Y-H, Ihlefeld JF, Erni R, Ederer C, Gopalan V, Chen LQ, Schlom DG, Spaldin NA, Martin LW, Ramesh R (2009) A strain-driven morphotropic phase boundary in BiFeO3. Science (New York, N.Y.). https://doi.org/10.1126/science.1177046

[32] Schader FH, Wang Z, Hinterstein M, Daniels JE, Webber KG (2016) Stress-modulated relaxor-to-ferroelectric transition in lead-free (Na1/2Bi1/2)TiO3−BaTiO3 ferroelectrics. Phys Rev B. https://doi.org/10.1103/PhysRevB.93.134111

[33] Prosandeev S, Wang D, Akbarzadeh AR, Dkhil B, Bellaiche L (2013) Field-induced percolation of polar nanoregions in relaxor ferroelectrics. Phys Rev Lett. https://doi.org/10.1103/PhysRevLett.110.207601

[34] Pramanick A, Dmowski W, Egami T, Budisuharto AS, Weyland F, Novak N, Christianson AD, Borreguero JM, Abernathy DL, Jørgensen MRV (2018) Stabilization of polar nanoregions in Pb-free ferroelectrics. Phys Rev Lett. https://doi.org/10.1103/PhysRevLett.120.207603

[35] Damjanovic D (2005) Contributions to the piezoelectric effect in ferroelectric single crystals and ceramics. J Am Ceram Soc. https://doi.org/10.1111/j.1551-2916.2005.00671.x

[36] Pramanick A, Damjanovic D, Daniels JE, Nino JC, Jones JL (2011) Origins of electro-mechanical coupling in polycrystalline ferroelectrics during subcoercive electrical loading. J Am Ceram Soc. https://doi.org/10.1111/j.1551-2916.2010.04240.x

[37] Schader FH, Isaia D, Weber M, Aulbach E, Webber KG (2018) High-temperature stress-dependent piezoelectric and dielectric coefficient of soft Pb(Zr, Ti)O3. J Mater Sci. https://doi.org/10.1007/s10853-017-1817-8

[38] Di Zhan, Xu Q, Huang D-P, Liu H-X, Chen W, Zhang F (2018) Contributions of intrinsic and extrinsic polarization species to energy storage properties of Ba 0.95 Ca 0.05 Zr 0.2 Ti 0.8 O 3 ceramics. J Phys Chem Solids. https://doi.org/10.1016/j.jpcs.2017.10.038

[39] Jo W, Dittmer R, Acosta M, Zang J, Groh C, Sapper E, Wang K, Rödel J (2012) Giant electric-field-induced strains in lead-free ceramics for actuator applications – status and perspective. J Electroceram. https://doi.org/10.1007/s10832-012-9742-3

[40] Schader FH, Aulbach E, Webber KG, Rossetti GA (2013) Influence of uniaxial stress on the ferroelectric-to-paraelectric phase change in barium titanate. J Appl Phys. https://doi.org/10.1063/1.4799581

[41] Fritz IJ (1978) Ultrasonic, dilatometric, and dielectric study of uniaxial-stress effects in a barium-calcium titanate ceramic. J Appl Phys. https://doi.org/10.1063/1.324658

[42] Humburg HI, Acosta M, Jo W, Webber KG, Rödel J (2015) Stress-dependent electromechanical properties of doped (Ba1−xCax)(ZryTi1−y)O3. J Eur Ceram Soc. https://doi.org/10.1016/j.jeurceramsoc.2014.10.016

[43] Zhang QM, Zhao J, Uchino K, Zheng J (1997) Change of the weak-field properties of Pb(ZrTi)O 3 piezoceramics with compressive uniaxial stresses and its links to the effect of dopants on the stability of the polarizations in the materials. J Mater Res. https://doi.org/10.1557/JMR.1997.0030

[44] Schader FH, Morozov M, Wefring ET, Grande T, Webber KG (2015) Mechanical stability of piezoelectric properties in ferroelectric perovskites. J Appl Phys. https://doi.org/10.1063/1.4919815

[45] Zhang QM, Zhao J (1999) Electromechanical properties of lead zirconate titanate piezoceramics under the influence of mechanical stresses. IEEE Trans Ultrason Ferroelect Freq Contr doi. https://doi.org/10.1109/58.808876

[46] Damjanovic D (1997) Stress and frequency dependence of the direct piezoelectric effect in ferroelectric ceramics. J Appl Phys. https://doi.org/10.1063/1.365981

[47] Damjanovic D, Demartin M (1996) The Rayleigh law in piezoelectric ceramics. J Phys D: Appl Phys. https://doi.org/10.1088/0022-3727/29/7/046

[48] Acosta M, Novak N, Rojas V, Patel S, Vaish R, Koruza J, Rossetti GA, Rödel J (2017) BaTiO 3 -based piezoelectrics:

Fundamentals, current status, and perspectives. Appl Phys Rev. https://doi.org/10.1063/1.4990046

[49] Ehmke MC, Schader FH, Webber KG, Rödel J, Blendell JE, Bowman KJ (2014) Stress, temperature and electric field effects in the lead-free (Ba, Ca)(Ti, Zr)O 3 piezo-electric system. Acta Mater. https://doi.org/10.1016/j.acta mat.2014.06.005

[50] Chaplya PM, Carman GP (2001) Dielectric and piezo-electric response of lead zirconate–lead titanate at high electric and mechanical loads in terms of non-180° domain wall motion. J Appl Phys. https://doi.org/10.1063/1. 1410330

[51] Dittmer R, Aulbach E, Jo W, Webber KG, Rödel J (2012) Large blocking force in Bi1/2Na1/2TiO3-based lead-free piezoceramics. Scripta Mater. https://doi.org/10.1016/j.scri ptamat.2012.03.031

[52] Ehmke MC (2014) Ferroelastic domains in lead-free bar-ium zirconate titanate - barium calcium titanate piezoce-ramics. Dissertation, Purdue University, West Lafayette, Indiana

[53] Ehmke MC, Glaum J, Hoffman M, Blendell JE, Bowman KJ (2013) In Situ X-ray Diffraction of Biased Ferroelastic Switching in Tetragonal Lead-free (1−x)Ba(Zr 0.2 Ti 0.8)O 3−x (Ba 0.7 Ca 0.3)TiO 3 Piezoelectrics. J Am Ceram Soc. https://doi.org/10.1111/jace.12424

[54] Guo H, Zhou C, Ren X, Tan X (2014) Unique single-domain state in a polycrystalline ferroelectric ceramic. Phys Rev B. https://doi.org/10.1103/PhysRevB.89.100104

[55] Coondoo I, Panwar N, Krylova S, Krylov A, Alikin D, Jakka SK, Turygin A, Shur VY, Kholkin AL (2021) Tem-perature-dependent Raman spectroscopy, domain mor-phology and photoluminescence studies in lead-free BCZT ceramic. Ceram Int. https://doi.org/10.1016/j.ceramint.202 0.09.137

[56] Stepkova V, Marton P, Hlinka J (2012) Stress-induced phase transition in ferroelectric domain walls of BaTiO3. J Phys Cond Matter Inst Phys J. https://doi.org/10.1088/ 0953-8984/24/21/212201

[57] Schader FH, Khakpash N, Rossetti GA, Webber KG (2017) Phase transitions in BaTiO 3 under uniaxial compressive stress: Experiments and phenomenological analysis. J Appl Phys. https://doi.org/10.1063/1.4976060

[58] Ehmke MC, Ehrlich SN, Blendell JE, Bowman KJ (2012) Phase coexistence and ferroelastic texture in high strain (1−x)Ba(Zr 0.2 Ti 0.8)O 3−x(Ba 0.7 Ca 0.3)TiO 3 piezoce-ramics. J Appl Phys. https://doi.org/10.1063/14730342

[59] Praveen JP, Karthik T, James AR, Chandrakala E, Asthana S, Das D (2015) Effect of poling process on piezoelectric properties of sol–gel derived BZT–BCT ceramics. J Eur Ceram Soc. https://doi.org/10.1016/j.jeurceramsoc.2014.12 .010

[60] Veber A, Cicconi MR, Reinfelder H, de Ligny D (2018) Combined Differential scanning calorimetry, Raman and Brillouin spectroscopies: A multiscale approach for mate-rials investigation. Anal Chimica Acta. https://doi.org/10. 1016/j.aca.2017.09.045

[61] Yan X, Zheng M, Gao X, Zhu M, Hou Y (2020) High-performance lead-free ferroelectric BZT–BCT and its application in energy fields. J Mater Chem C. https://doi. org/10.1039/D0TC03461D

[62] Acosta M, Khakpash N, Someya T, Novak N, Jo W, Nagata H, Rossetti GA, Rödel J (2015) Origin of the large piezo-electric activity in (1–x)Ba(Zr0.2Ti0.8)O3–x(Ba0.7Ca0.3)-TiO3 ceramics. Phys Rev B. https://doi.org/10.1103/Ph ysRevB.91.104108

[63] Acosta M, Novak N, Jo W, Rödel J (2014) Relationship between electromechanical properties and phase diagram in the Ba(Zr0.2Ti0.8)O3–x(Ba0.7Ca0.3)TiO3 lead-free piezoceramic. Acta Mater. https://doi.org/10.1016/j.actama t.2014.07.058

[64] Liu G, Zhang S, Jiang W, Cao W (2015) Losses in ferro-electric materials. Mater Sci Eng R Rep. https://doi.org/10. 1016/j.mser.2015.01.002

[65] Cordero F, Craciun F, Dinescu M, Scarisoreanu N, Galassi C, Schranz W, Soprunyuk V (2014) Elastic response of (1–x)Ba(Ti 0.8 Zr 0.2)O 3–x (Ba 0.7 Ca 0.3)TiO 3 (x = 0.45–0.55) and the role of the intermediate orthorhombic phase in enhancing the piezoelectric coupling. Appl Phys Lett. https://doi.org/10.1063/1.4903807

[66] Sundar V, Newnham RE (1992) Electrostriction and polarization. Ferroelectrics. https://doi.org/10.1080/ 00150199208230043

[67] Weaver PM, Cain MG, Stewart M (2010) Temperature dependence of high field electromechanical coupling in ferroelectric ceramics. J Phys D: Appl Phys. https://doi.org/ 10.1088/0022-3727/43/16/165404

[68] Dittmer R, Webber KG, Aulbach E, Jo W, Tan X, Rödel J (2013) Optimal working regime of lead–zirconate–titanate for actuation applications. Sens Actuators, A. https://doi. org/10.1016/j.sna.2012.09.015

[69] Anton E-M, Jo W, Damjanovic D, Rödel J (2011) Deter-mination of depolarization temperature of (Bi 1/2 Na 1/2)TiO 3 -based lead-free piezoceramics. J Appl Phys. h ttps://doi.org/10.1063/1.3660253

[70] Zhang XL, Chen ZX, Cross LE, Schulze WA (1983) Dielectric and piezoelectric properties of modified lead titanate zirconate ceramics from 42 to 300 K. J Mater Sci. h ttps://doi.org/10.1007/BF00551962

[71] Merz WJ (1950) The effect of hydrostatic pressure on the curie point of barium titanate single crystals. Phys Rev. https://doi.org/10.1103/PhysRev.78.52

[72] Forsbergh PW (1954) Effect of a two-dimensional pressure on the curie point of barium titanate. Phys Rev. https://doi.org/10.1103/PhysRev.93.686

[73] Samara GA (1966) Pressure and temperature dependences of the dielectric properties of the perovskites BaTi O3 and SrTi O3. Phys Rev. https://doi.org/10.1103/PhysRev.151.378

[74] Shannon RD (1976) Revised effective ionic radii and systematic studies of interatomic distances in halides and chalcogenides. Acta Cryst A. https://doi.org/10.1107/S0567739476001551

[75] Zakhozheva M, Schmitt LA, Acosta M, Guo H, Jo W, Schierholz R, Kleebe H-J, Tan X (2015) Wide compositional range in situ electric field investigations on lead-free Ba(Zr0.2Ti0.8)O3–x(Ba0.7Ca0.3)TiO3 Piezoceramic. Phys Rev Appl. https://doi.org/10.1103/PhysRevApplied.3.064018

[76] Di Z, Xu Q, Huang D-P, Liu H-X, Chen W, Zhang F (2016) Dielectric nonlinearity and electric breakdown behaviors of Ba0.95Ca0.05Zr0.3Ti0.7O3 ceramics for energy storage utilizations. J Alloys Comp. https://doi.org/10.1016/j.jallcom.2016.04.317

[77] Yu Z, Ang C, Guo R, Bhalla AS (2002) Dielectric properties and high tunability of Ba(Ti0.7Zr0.3)O3 ceramics under dc electric field. Appl Phys Lett. https://doi.org/10.1063/1.1498496

[78] Li Z, Fan H (2009) Polaron relaxation associated with the localized oxygen vacancies in Ba0.85Sr0.15TiO3 ceramics at high temperatures. J Appl Phys. https://doi.org/10.1063/1.3211308

[79] Merselmiz S, Hanani Z, Mezzane D, Razumnaya AG, Amjoud M, Hajji L, Terenchuk S, Rožič B, Luk'yanchuk IA, Kutnjak Z (2021) Thermal-stability of the enhanced piezoelectric, energy storage and electrocaloric properties of a lead-free BCZT ceramic. RSC Adv. https://doi.org/10.1039/D0RA09707A

[80] Hanani Z, Mezzane D, Amjoud M, Razumnaya AG, Fourcade S, Gagou Y, Hoummada K, El Marssi M, Goune M (2019) Phase transitions, energy storage performances and electrocaloric effect of the lead-free Ba0.85Ca0.15Zr0.10Ti0.90O3 ceramic relaxor. J Mater Sci Mater Electron. https://doi.org/10.1007/s10854-019-00946-5

[81] Hamza A, Benabdallah F, Kallel I, Seveyrat L, Lebrun L, Khemakhem H (2018) Effect of rare-earth substitution on the electrical properties and Raman spectroscopy of BCTZ ceramics. J Alloy Compd. https://doi.org/10.1016/j.jallcom.2017.11.351

[82] Merz WJ (1949) The electric and optical behavior of BaTi O3 single-domain crystals. Phys Rev. https://doi.org/10.1103/PhysRev.76.1221

[83] Picht G, Webber KG, Zhang Y, Kungl H, Damjanovic D, Hoffmann MJ (2012) Critical mechanical and electrical transition behavior of BaTiO 3 The observation of mechanical double loop behavior. J Appl Phys. https://doi.org/10.1063/1.4767059

[84] Guo H, Voas BK, Zhang S, Zhou C, Ren X, Beckman SP, Tan X (2014) Polarization alignment, phase transition, and piezoelectricity development in polycrystalline 0.5Ba(Zr0.2Ti0.8)O3–0.5(Ba0.7Ca0.3)TiO3. Phys Rev B. https://doi.org/10.1103/PhysRevB.90.014103

[85] Zakhozheva M, Schmitt LA, Acosta M, Jo W, Rödel J, Kleebe H-J (2014) In situ electric field induced domain evolution in Ba(Zr 0.2 Ti 0.8)O 3–0.3(Ba 0.7 Ca 0.3)TiO 3 ferroelectrics. Appl Phys Lett. https://doi.org/10.1063/1.4896048

[86] Ghita M, Fornari M, Singh DJ, Halilov SV (2005) Interplay between A -site and B -site driven instabilities in perovskites. Phys Rev B. https://doi.org/10.1103/PhysRevB.72.054114

[87] Zuo R, Rodel J, Chen R, Li L (2006) Sintering and electrical properties of lead-free Na0.5K0.5NbO3 Piezoelectric Ceramics. J Am Ceramic Soc. https://doi.org/10.1111/j.1551-2916.2006.00991.x

[88] Martin A, Khansur NH, Eckstein U, Riess K, Kakimoto K, Webber KG (2020) High temperature piezoelectric response of polycrystalline Li-doped (K, Na)NbO 3 ceramics under compressive stress. J Appl Phys. https://doi.org/10.1063/1.5134554

[89] Wu M, Fang L, Liu L, Zhou X, Huang Y, Li Y (2012) Diffusion phase transition and ferroelectric properties of 0.92K0.5Na0.5NbO3–(0.08–x)Bi0.5Li0.5TiO3–xBaZrO3 ceramics. Mater Chem Phys. https://doi.org/10.1016/j.matchemphys.2011.12.051

[90] Wang R, Wang K, Yao F, Li J-F, Schader FH, Webber KG, Jo W, Rödel J (2015) Temperature stability of lead-free niobate piezoceramics with engineered morphotropic phase boundary. J Am Ceram Soc. https://doi.org/10.1111/jace.13604

[91] Hayward SA, Salje EKH (2002) The pressure temperature phase diagram of BaTiO 3 a macroscopic description of the low-temperature behaviour. J Phys Condens Matter. https://doi.org/10.1088/0953-8984/14/36/101

[92] Buscaglia V, Tripathi S, Petkov V, Dapiaggi M, Deluca M, Gajović A, Ren Y (2014) Average and local atomic-scale structure in BaZrxTi(1–x)O3 (x = 0.10, 0.20, 0.40)

ceramics by high-energy x-ray diffraction and Raman spectroscopy. J Phys Cond Matter Inst Phys J. https://doi.org/10.1088/0953-8984/26/6/065901

[93] Deluca M, Fukumura H, Tonari N, Capiani C, Hasuike N, Kisoda K, Galassi C, Harima H (2011) Raman spectroscopic study of phase transitions in undoped morphotropic PbZr1−xTixO3. J Raman Spectrosc. https://doi.org/10.1002/jrs.2714

[94] Gillet P, Guyot F, Price GD, Tournerie B, Le Cleach A (1993) Phase changes and thermodynamic properties of CaTiO3. Spectroscopic data, vibrational modelling and some insights on the properties of MgSiO3 perovskite. Phys Chem Minerals. https://doi.org/10.1007/BF00200118

[95] Williams Q, Jeanloz R, McMillan P (1987) Vibrational spectrum of MgSiO 3 perovskite: Zero-pressure Raman and mid-infrared spectra to 27 GPa. J Geophys Res. https://doi.org/10.1029/JB092iB08p08116

[96] Ikegami S (1964) Raman spectrum of BaTiO 3. J Phys Soc Jpn. https://doi.org/10.1143/JPSJ.19.46

[97] Freire K (1988) Lattice dynamics of crystals with tetragonal BaTiO3 structure. Phys Rev B: Condens Matter. https://doi.org/10.1103/PhysRevB.37.2074

[98] Jayakrishnan AR, Alex KV, Thomas A, Silva J, Kamakshi K, Dabra N, Sekhar KC, Agostinho Moreira J, Gomes M (2019) Composition-dependent xBa(Zr02Ti08)O3-(1−x)(Ba07Ca03)TiO3 bulk ceramics for high energy storage applications. Ceramics Int. https://doi.org/10.1016/j.ceramint.2018.11.250

[99] Pytte E (1972) Theory of perovskite ferroelectrics. Phys Rev B. https://doi.org/10.1103/PhysRevB.5.3758

[100] Jalalian A, Grishin AM, Wang X, Dou SX (2012) Fabrication of Ca, Zr doped BaTiO3 ferroelectric nanofibers by electrospinning. Phys Status Solidi C. https://doi.org/10.1002/pssc.201200010

[101] Puli VS, Kumar A, Chrisey DB, Tomozawa M, Scott JF, Katiyar RS (2011) Barium zirconate-titanate/barium calcium-titanate ceramics via sol–gel process: novel high-energy-density capacitors. J Phys D: Appl Phys. https://doi.org/10.1088/0022-3727/44/39/395403

[102] Frey P (1996) Grain-size effect on structure and phase transformations for barium titanate. Phys Rev B: Condens Matter. https://doi.org/10.1103/PhysRevB.54.3158

[103] Pokorný J, Pasha UM, Ben L, Thakur OP, Sinclair DC, Reaney IM (2011) Use of Raman spectroscopy to determine the site occupancy of dopants in BaTiO 3. J Appl Phys. https://doi.org/10.1063/1.3592192

[104] Abdessalem MB, Aydi S, Aydi A, Abdelmoula N, Sassi Z, Khemakhem H (2017) Polymorphic phase transition and morphotropic phase boundary in Ba1−x Ca x Ti1−y Zr y O3 ceramics. Appl Phys A. https://doi.org/10.1007/s00339-017-1196-7

[105] Shi J, Zhu R, Liu X, Fang B, Yuan N, Ding J, Luo H (2017) Large electrocaloric effect in lead-free (Ba0.85Ca0.15)(Zr0.1Ti0.9)O3 ceramics prepared via citrate route. Mater (Basel, Switzerland). https://doi.org/10.3390/ma10091093

[106] Zhang M-H, Wang K, Zhou J-S, Zhou J-J, Chu X, Lv X, Wu J, Li J-F (2017) Thermally stable piezoelectric properties of (K, Na)NbO3-based lead-free perovskite with rhombohedral-tetragonal coexisting phase. Acta Mater. https://doi.org/10.1016/j.actamat.2016.10.011

[107] Zhao C, Wu H, Li F, Cai Y, Zhang Y, Song D, Wu J, Lyu X, Yin J, Xiao D, Zhu J, Pennycook SJ (2018) Practical high piezoelectricity in barium titanate ceramics utilizing multiphase convergence with broad structural flexibility. J Am Chem Soc. https://doi.org/10.1021/jacs.8b07844

[108] Joshi UA, Yoon S, Baik S, Lee JS (2006) Surfactant-free hydrothermal synthesis of highly tetragonal barium titanate nanowires: a structural investigation. J Phys Chem B. https://doi.org/10.1021/jp0600110

[109] Karan NK, Katiyar RS, Maiti T, Guo R, Bhalla AS (2009) Raman spectral studies of Zr 4+ -rich BaZr x Ti 1−x O 3 (05⩽ x ⩽100) phase diagram. J Raman Spectrosc. https://doi.org/10.1002/jrs.2134

[110] Dobal PS, Dixit A, Katiyar RS, Yu Z, Guo R, Bhalla AS (2001) Micro-Raman scattering and dielectric investigations of phase transition behavior in the BaTiO3–BaZrO3 system. J Appl Phys. https://doi.org/10.1063/1.1369399